ACS APPLIED MATERIALS & INTERFACES

www.acsami.org

Research Article

Facile Production of Graphenic Microsheets and Their Assembly via Water-Based, Surfactant-Aided Mechanical Deformations

Mohammed AlAmer, Somayeh Zamani, Kristi Fok, Aishwarya Satish, Ae Ran Lim, and Yong Lak Joo*

Cite This: https://dx.doi.org/10.1021/acsami.9b22824

Read Online

ACCESS | Metrics & More | Article Recommendations | Supporting Information

ABSTRACT: Expandable graphite (EG) and few-layer graphene (FLG) have proven to be instrumental materials for various applications. The production of EG and FLG has been limited to batch processes using numerous intercalating agents, especially organic acids. In this study, a Taylor−Couette reactor (TCR) setup is used to expand and exfoliate natural graphite and produce a mixture of EG and FLG in aqueous solutions using an amphiphilic dispersant and a semiflexible stabilizer. Laminar Couette flow structure and high shear rates are achieved via the rotation of the outer cylinder while the inner cylinder is still, which circumvents vortex formation because of the suppression of centrifugal forces. Our results reveal that the level of expansion and exfoliation using an aqueous solution and a TCR is comparable to that using commercial EG (CEG) synthesized by intercalating sulfuric acid. More importantly, the resultant EG and FLG flakes are more structurally homogeneous than CEG, the ratio of FLG to EG increases with increasing shearing time, and the produced FLG sheets exhibit large lateral dimensions (>10 μm). The aqueous solutions of EG and FLG are wet-spun to produce ultralight fibers with a bulk density of 0.35 g/cm^3. These graphene fibers exhibit a mechanical strength of 0.5 GPa without any modification or thermal treatment, which offers great potential in light-weight composite applications.

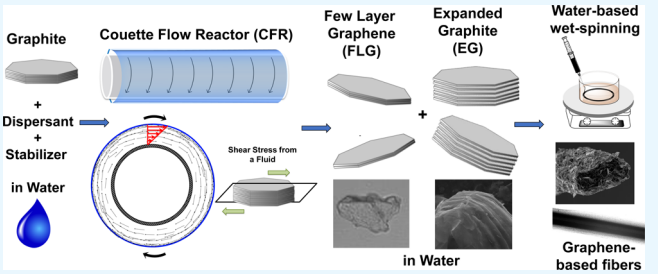

KEYWORDS: *graphene, graphite, Taylor−Couette, exfoliation, expansion, fiber*

1. INTRODUCTION

Graphene, a two-dimensional material that consists of a single atomic layer of sp^2-bonded carbon atoms arranged in a honeycomb lattice, has attracted tremendous attention because of its remarkable electronic,[1] mechanical,[2] and thermal[3] properties. It is considered the parent material for many carbon allotropes, including fullerene (0D), carbon nanotubes (1D), and graphite (3D).[4] As a result of its large theoretical surface area (>2600 m^2/g)[5] and ease of surface modification,[6] graphene could be used as a two-dimensional coating material to enhance the properties of the underlying material.[7,8] Graphene-based materials are being investigated for potential use in numerous applications, including batteries,[9] supercapacitors,[10] fuel cells,[11] and transistors.[12]

A number of graphene synthesis methods have been reported, including chemical vapor deposition,[13] epitaxial growth on silicon carbide substrates,[14] micromechanical exfoliation,[15] and thermal and chemical reduction of graphene oxide (GO).[16,17] Because the production of GO is diffusion-limited, a Taylor−Couette reactor (TCR) with a rotating inner cylinder was used in batch to produce multilayered GO sheets within 30 min. The rotation of the inner cylinder in the TCR generates Taylor vortices, which enhances the diffusion of oxidizing agents into the interlayer spacing in between graphene sheets in graphite particles.[18] In our previous study, a continuous TCR system was deployed and the Taylor vortex flow regime resulted in uniformly structured graphite oxide sheets with low defect amounts and high yields.[19] High shear-induced exfoliation of graphite into high-quality graphene was achieved using an inner-rotating TCR setup using natural graphite and organic solvents. Turbulent Taylor vortices were used to induce high wall shear stress and pressure to produce few-layer graphene (FLG) sheets with a low degree of defects at ∼5% yield.[20] Conventional TCR setups consist of two coaxial cylinders with the inner cylinder rotating while the outer cylinder is still, creating toroidal, or Taylor, vortices that enhance the mixing of the reaction medium.[21,22] Other TCR setups could include the rotation of the outer cylinder while the inner cylinder is still, which generates Couette flow without vortex formation because of the absence of centrifugal forces acting on the reaction medium. While co- and counter-rotating cylinders in the TCR could generate a number of flow vortex structures, the rotating outer cylinder and slowly rotating inner

Received: December 17, 2019
Accepted: January 29, 2020
Published: January 29, 2020

cylinder could induce high wall shear stress on the reaction medium while maintaining a Couette flow regime (CFR).[23]

Expandable graphite (EG), or the graphite intercalation compound, is an essential precursor for the production of expanded graphite, which consists of stacked, flexible graphene sheets capable of expanding upon heating. Graphite intercalation is achieved using an intercalant material, which is inserted between the graphene sheets. The resulting graphite material comprises hybrid properties that are a function of the intercalating material.[24] Intercalation affects the physical and chemical properties of graphite and results in low yields of exfoliated graphene sheets.[25] Numerous intercalants have been used to intercalate graphite materials including halogens,[25,26] alkali metals,[27,28] sulfate,[29−31] nitrate,[25,30,32] organic acids,[28,29,33] and metal oxides.[32] EG can also be produced with ultrasound irradiation using an ultrasonic solvent.[33] EG can be exfoliated resulting in single graphene sheets upon exposure to heat. High temperatures cause the expansion and gasification of the intercalating agents, resulting in sufficient pressure to break the van der Waals forces that hold the graphene sheets together.[34] Other exfoliation methods that use EG as a starting material include microwave irradiation using sulfuric acid[35] and ammonia[36] and solvothermal-assisted exfoliation in acetonitrile.[37] Expanded graphite has been widely used as high-performance sealing gaskets, fire extinguisher agents, thermal insulators, conductive resin composites, electrodes, fibers, and in more applications.[38]

Graphene fiber (GF) has raised a considerable attention because of its extraordinary inherent mechanical and electrical properties. Ever since GF was first produced, novel processes have been investigated to fabricate GF from graphite.[39] However, these processes usually included severe chemical or thermal modifications.[40] Cong and his co-workers used wet-spinning assembly to fluidly spin GO suspensions into macroscopic GF in a low-cost, effective, and scalable manner. The assembly of GF was performed under the electrostatic interactions of the opposite charges present in the wet-spinning coagulation bath.[41] The fabrication of GF is affected by the crumpled nature of graphene and low bending rigidity. This leads to irregularly folded structures and creased regions, altering the physical and chemical properties of the planar precursor.[42,43] Other folding techniques can be employed on 2D materials to produce three-dimensional shapes including capillary origami[44] and nanodroplet-guided folding.[45]

In the current study, we report the synthesis of EG and FLG using simple shearing in the TCR with a dimensionless control parameter, namely, the Reynolds number of the outer rotating cylinder. The results will be discussed in terms of expansion of the interlayer spacing in between graphene sheets, structural defect content, and exfoliation levels. The reported novel expansion and exfoliation method is performed in an aqueous solution that contains a benign, amphiphilic dispersant and a semiflexible stabilizing agent instead of a highly acidic solution. We will demonstrate how maintaining the simple shear flow structure in the TCR by rotating the outer cylinder, while the inner cylinder is still, resulted in a structurally uniform EG and FLG product that is comparable to commercial EG (CEG), and the produced sheets exhibit large lateral dimensions that exceed 10 μm. We also demonstrate how longer shearing times in the TCR could result in structural defects on the graphene sheets. In addition, we demonstrate how fibers could be fabricated from EG and FLG aqueous solutions using a wet-spinning setup. We finally demonstrate how the effective, low-cost spinning process results in ultralightweight graphenic fibers that exhibit very high mechanical properties.

2. EXPERIMENTAL SECTION

2.1. Materials. Natural graphite powders (3061, 180−425 mesh) and CEG (3772, 180−425 mesh) were obtained from Asbury Carbon. Xanthan gum (CAS# 11138-66-2) and ethanol were purchased from VWR and used as provided as a stabilizing agent. Pluronic F127 (CAS# 9003-11-6), PEO/PPO/PEO = 100:65:100, was obtained from BASF and used as provided as a dispersant. Cetyl trimethylammonium bromide (CTAB) (CAS# 57-09-0) was purchased from Sigma. Deionized (DI) water was used during all of the syntheses.

2.2. Experimental Setup. The experimental setup of the TCR shown in Figure 1 consisted of two coaxial cylinders, with the outer

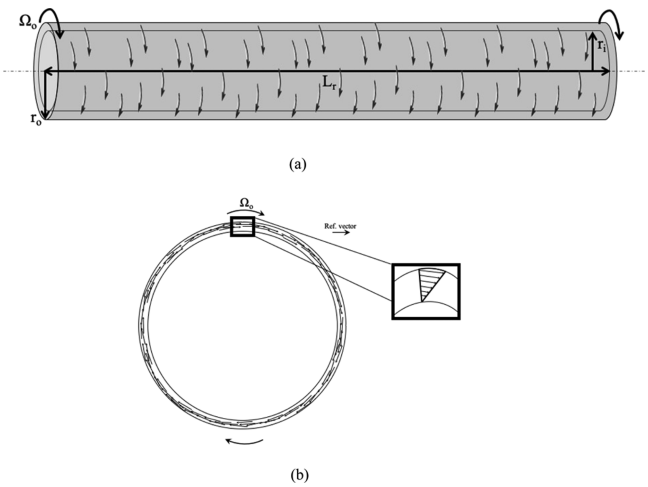

Figure 1. Schematic of a Couette flow reactor setup: (a) side view of the reactor with the physical dimensions and (b) cross-sectional view of the reactor.

one (plexiglass) rotating while the inner one (stainless steel) is still. The physical specifications of the TCR used in the current study are displayed in Table 1, where r_o and r_i are the outer and inner cylinder

Table 1. Dimensions of the TCR

r_i (cm)	r_o (cm)	d ($r_o - r_i$) (cm)	L_r (cm)
2.46	2.54	0.08	30.48

radii, respectively, d is the corresponding gap width, and L_r is the length of the TCR. The outer cylinder rotation rate is controlled using a phase inverter, connected to a motor drive that provides rotation rates in the range of 10−1800 rpm. The TCR system is driven through the rotation of the outer cylinder, which is quantified in the dimensional form of the outer cylinder's angular velocity Ω_o and in the dimensionless form by the Reynolds number Re_o using the kinematic viscosity υ of the Newtonian fluid between the two cylinders, which is calculated using the following equation

$$Re_o = \frac{r_o \Omega_o d}{\upsilon} \quad (1)$$

2.3. EG and FLG Synthesis. Natural graphite (20 g) was suspended in DI water (200 mL), and the obtained solution is stirred for 10 min. Then, Xanthan gum (0.54 g) is slowly added, and the stirring continued for 10 min. Pluronic F127 (0.6 g) is slowly added to the mixture, and the stirring continued for 10 min.[46] The mixture solution is introduced into the gap between the two cylinders in a stationary TCR. The rotation speed is fixed at 1500 rpm. The rotation of the outer cylinder while the inner cylinder is stationary induces

https://dx.doi.org/10.1021/acsami.9b22824
ACS Appl. Mater. Interfaces XXXX, XXX, XXX−XXX

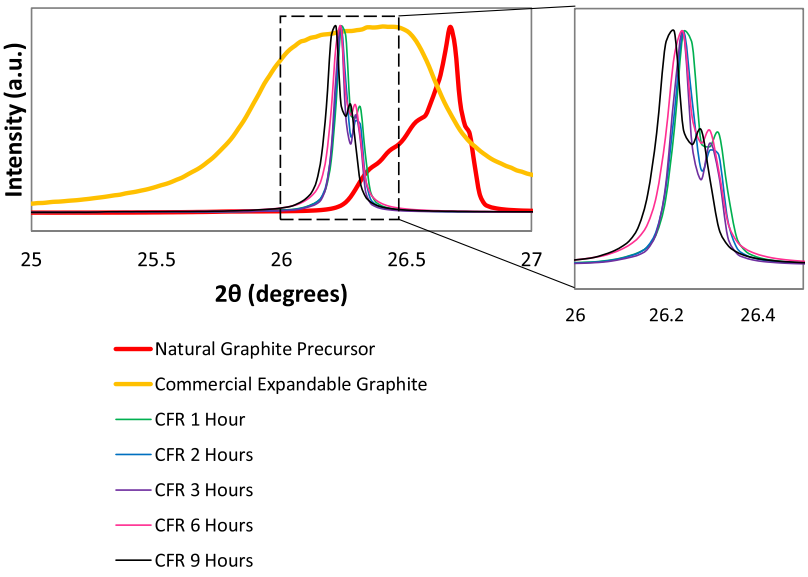

Figure 2. XRD patterns of natural graphite, CEG, and synthesized EG/FLG samples in the CFR with respect to shearing time.

high wall shear stress (shear rate ≈ 5300 s^{-1}), which eases the penetration of the dispersant particles into the interlayer spacing of the graphene sheets. The shearing time in the TCR is varied between 1 and 9 h. The observed color of the mixture is dark gray, and underexpanded natural graphite flakes are suspended in the solution. The resulting mixture is centrifuged at 2000 rpm for 90 min, where the underexpanded natural graphite flakes sediment. Air-controlled electrospray is applied for directly depositing the centrifugate on silicon wafers (25.4 mm diameter, 400 μm thickness, University Wafer).[9] The electrospray is performed under ambient conditions using a Harvard Apparatus PHD 2000 infusion syringe pump with a coaxial needle set. EG/FLG solution is supplied through the inner 17 G needle, and air is supplied through the outer 12 G needle. The working voltage is set at 25 kV, the working distance is set at 15 cm, the solution feeding rate is set at 0.05 mL min^{-1}, the air pressure is set at 20 psi, and a total of 2 mL of the sprayed material is used. The sprayed wafers are dried using a vacuum oven at 45 °C.

2.4. GF Fabrication. The aqueous EG/FLG solution is loaded in a plastic syringe (5 mL) and injected into a rotating CTAB coagulation bath (0.5 wt % in DI water/ethanol = 1:1) using a 22 G needle with an infusion rate of 0.75 mL min^{-1} and a rotation speed of 15 rpm. Charge neutralization between the graphene sheets and the coagulant in the wet-spinning process weakens the electrostatic repulsions that lead to the curling and folding of the edges of the sheets. The obtained fibers are kept in the coagulation bath for 30 min and then transferred into a washing bath (DI water/ethanol = 1:1) for 60 min. The fibers are then dried at room temperature.

2.5. Characterization. For sample characterization, the collected EG/FLG solution is centrifuged at 2000 rpm for 90 min to allow for the sedimentation of underexpanded natural graphite particles. The centrifugate is collected and electrosprayed on silicon wafers. X-ray diffraction (XRD) patterns of the electrosprayed EG/FLG samples are determined using a D8 ADVANCE ECO powder diffractometer (Bruker Corporation) using a high-brilliance 1 kW X-ray source. The microstructures of the graphene sheets are investigated using inVia confocal Raman microscopy (Renishaw) with a 488 nm laser beam. Scanning electron microscopy (SEM) is performed using a MIRA 3 FEG-SEM (Tescan). Optical microscope images of EG/FLG solutions are obtained using a 40×–2000× Professional Infinity trinocular compound microscope with a 14 MP camera (AmScope). The zeta potential values of the EG/FLG solutions are determined using a Zetasizer Nano S (Malvern). Mechanical properties of the as-spun EG/FLG fibers are analyzed by dynamic mechanical analysis.

3. RESULTS AND DISCUSSION

In the current TCR system, the outer cylinder rotation and the idle inner cylinder resulted in the continuous formation of a CFR. Couette flow is a simple, stable shearing flow regime characterized by the absence of axisymmetric instabilities and centrifugal forces that form Taylor vortices in conventional TCR setups with the rotating inner cylinder.[23]

3.1. XRD Analysis. XRD analysis was used to study the effect of the CFR on the expansion of graphene sheets and the structural crystallinity of the synthesized samples. Figure 2 compares XRD patterns for the samples with respect to shearing time in the TCR. The main graphenic XRD peak corresponds to the interlayer spacing according to Bragg's law. Natural graphite has the main peak at 26.66° of 2θ corresponding to an interlayer spacing of 3.34 Å. We note that CEG has a broad peak expanding between ∼25 and ∼28°. The broad CEG XRD spectrum can be deconvoluted to a number of smaller peaks that correspond to interlayer spacing spanning between ∼3.18 and ∼3.55 Å. This confirms the structural inhomogeneity in the CEG sample that contains graphite flakes with varying interlayer spacing. After expanding natural graphite to synthesize EG and FLG, the main XRD peak shifts toward the left with a longer residence time in the TCR. The much narrower XRD peaks suggest the structural homogeneity in the synthesized EG and FLG samples. All XRD peaks are narrow-shaped, suggesting that the stacking structure of the natural graphite precursor is preserved. Figure 3 shows the increasing interlayer spacing between graphene sheets from ∼3.34 to ∼3.40 Å based on Bragg's law. The

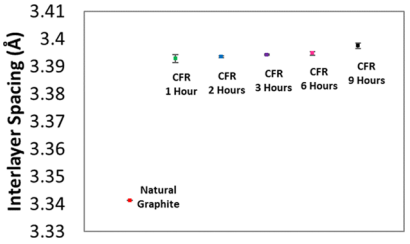

Figure 3. Interlayer spacing of the EG/FLG samples.

https://dx.doi.org/10.1021/acsami.9b22824
ACS Appl. Mater. Interfaces XXXX, XXX, XXX−XXX

increase in interlayer spacing is attributed to the intercalation of the dispersing and stabilizing agents in between the graphene sheets in the graphite structure.

3.2. Raman Spectroscopy. Raman spectroscopy was used to investigate structural defects on the synthesized graphene sheets. The energy shift caused by laser excitation creates main Raman peak positions: D band (1350 cm^{-1}), G band (1570 cm^{-1}), and 2D band (2700 cm^{-1}). The D band is a defect-activated peak that corresponds to sp^3-defects or vacancy-type defects.[47] The G band position shifts to a higher wavelength (1600 cm^{-1}) in the presence of oxygenated functional groups on the graphene structure. The absence of oxidation in this application suggests that all defect-activated peaks correspond to vacancy-type defects. The 2D band increases in intensity and broadens in shape with increasing exfoliation levels. Exposing natural graphite flakes to the strong Couette fluid flow results in structural changes in the graphite lattice, which yields a higher intensity of the D band. Figure 4 shows the

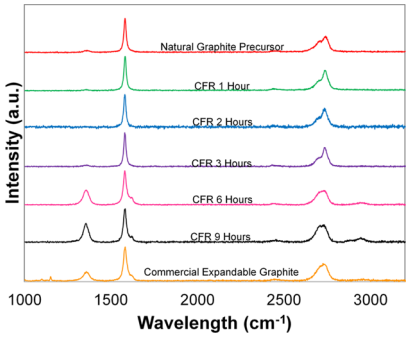

Figure 4. Raman spectroscopy of natural graphite, synthesized EG/FLG samples in the CFR with respect to shearing time, and CEG.

Raman spectra (E_{laser} = 488 nm) of the natural graphite precursor, CEG, and TCR-synthesized EG/FLG samples. It shows that the natural graphite precursor and the synthesized EG/FLG samples with the shearing time between 1 and 3 h exhibit almost no defects on the graphene sheets. Raman spectra of the EG/FLG samples with 6 and 9 h shearing time and the CEG reveal the presence of structural defects on the graphene sheets. The $I_{(D)}/I_{(G)}$ ratio is used to determine the defect level and increases with increasing defects. The $I_{(D)}/I_{(G)}$ ratio of natural graphite (~0.04) indicates the low defect level in graphite particles. We note that the $I_{(D)}/I_{(G)}$ ratio of the synthesized EG/FLG samples at shearing times between 1 and 3 h remains at the same level as the $I_{(D)}/I_{(G)}$ ratio of the natural graphite precursor. The $I_{(D)}/I_{(G)}$ ratio starts increasing after 6 h ($I_{(D)}/I_{(G)}$ = ~0.48) and 9 h ($I_{(D)}/I_{(G)}$ = ~0.48) because of the exposure of the high shear rate at extended shearing times in the TCR. The defect levels after 6 and 9 h are reportedly higher than CEG ($I_{(D)}/I_{(G)}$ = ~0.18).

3.3. Zeta Potential. Zeta potential represents the potential difference between the stationary double layer attached to the dispersed particle and the mobile dispersion medium. Zeta potential values reflect the short- and long-term stability of dispersions. Solutions with high zeta potential, positive or negative, are electrically stabilized. The stability in the EG/FLG solution depends on the balance between two counteracting forces: van der Waals attractive forces and electrical double-layer repulsive forces. If the zeta potential of an emulsion is high, the repulsive forces exceed the attractive forces, which results in a relatively stable system. Figure 5

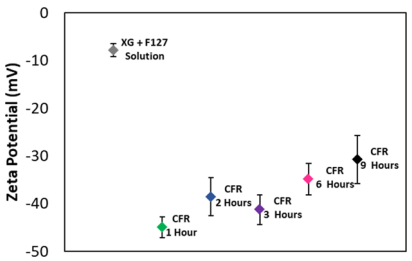

Figure 5. Zeta potential of Xanthan gum and Pluronic F127 solution and synthesized EG/FLG samples in the CFR with respect to shearing time.

depicts the zeta potentials of the solutions where the pH of the synthesized EG/FLG solutions was 7.64 ± 0.13 (see the Supporting Information). It shows that the zeta potential is comparable in synthesized EG/FLG samples with the shearing time between 1 and 3 h. We note a decrease in the magnitude of the zeta potential in samples with shearing times of 6 and 9 h, which suggests the increased concentration of exfoliated graphene sheets (e.g., FLG) and the lack of repulsive forces displayed by the EG.

3.4. Morphological Characterization. SEM micrographs of CEG and synthesized EG flakes are shown in Figure 6. The representative micrographs showed how the stacked morphology of the graphite layers in the synthesized EG samples has expanded and the layer distance has been enlarged. Figure 6a is comparable to Figure 6b–f in terms of the expanded graphene-layered structure (see the Supporting Information for SEM micrograph of NG). This confirms the morphological similarity between CEG and the synthesized EG samples, which includes well-marked separation of the expanded layers. The synthesized EG samples were further diluted in DI water, and the flake size distribution was investigated using optical microscopy (see the Supporting Information). The ratio of EG to exfoliated graphene sheets in EG/FLG samples is determined using optical microscopy images and edge-detection using an in-house-developed MATLAB code. Each detected particle is classified as EG or FLG based on the brightness of the particle. Stacked graphitic particles are observed to be darker in color under the microscope in comparison to FLG particles. The number of particles in each classification is used to determine the ratio of EG particles to graphene sheets according to the following equation

$$\text{Ratio} = \frac{\text{number of EG particles}}{\text{number of FLG particles}} \quad (2)$$

It can be seen in Figure 7 that there is a decrease in the EG/FLG ratio as the shearing time increases, which suggests the increase in the degree of exfoliation with longer shearing times.

3.5. Fiber Fabrication. Water-based wet spinning was used to fabricate fibers from CEG and EG/FLG solutions obtained from natural graphite. The initial CEG dispersion contains smaller flakes than natural graphite dispersion as illustrated in optical microscopy images (see the Supporting Information), and wet spinning was not a viable option. Further expansion and exfoliation in the TCR for 1 h rendered the solution spinnable, and CEG fibers were fabricated from 10 to 15% solutions. All samples were rested overnight in order for the larger particles to sediment, and the upper solution was then used for fiber fabrication. The spun solution contained 60

https://dx.doi.org/10.1021/acsami.9b22824
ACS Appl. Mater. Interfaces XXXX, XXX, XXX−XXX

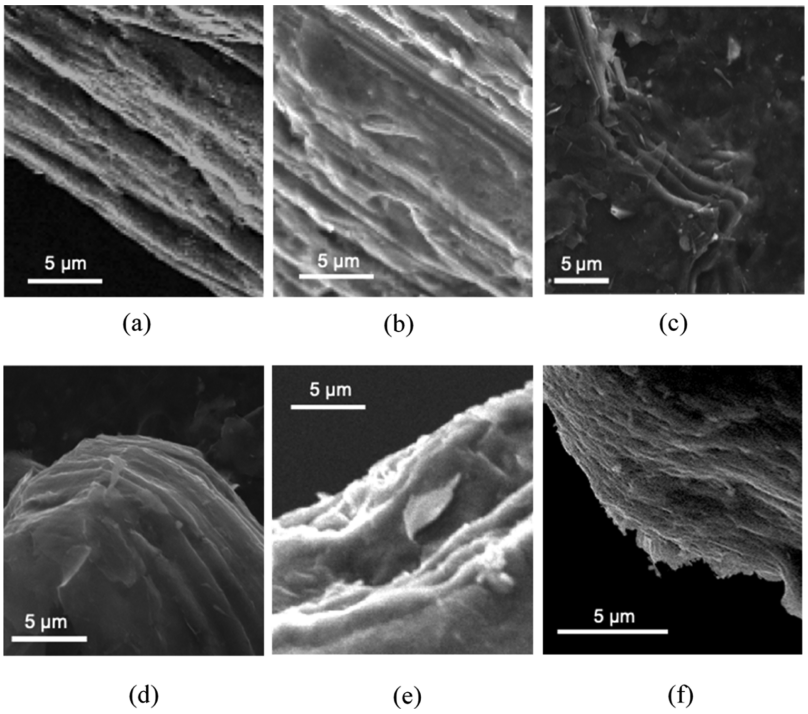

Figure 6. SEM micrographs of (a) CEG, (b) CFR 1 h, (c) CFR 2 h, (d) CFR 3 h, (e) CFR 6 h, and (f) CFR 9 h.

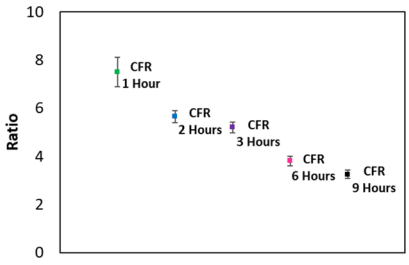

Figure 7. Ratio of EG to exfoliated graphene sheets in synthesized EG/FLG samples in the CFR with respect to shearing time.

and 80 wt % of the flakes for CEG and EG/FLG fibers, respectively.

Fiber morphology and mechanical properties were studied for all fabricated fibers. Figure 8 illustrates the tensile strength of different fibers. Both 10 and 15% CEG fibers were weak in terms of tensile strength and Young's modulus in comparison to EG/FLG fibers. This further shows the importance of the flake size on the macroscopic fiber properties, where larger flakes in EG/FLG dispersions led to stronger fibers. EG/FLG fibers revealed higher tensile strengths, and Young's modulus could reach as high as 35 GPa. Longer shearing times in the TCR affected the mechanical strength of the resulting fibers which peaked for fibers from 3 h of shearing time, followed by significant decreases with further increasing shearing time. It shows that 3 h of shearing time is optimal to expand graphite sheets and interlink the suspended particles. Additionally, the presence of structural defects, increased exfoliation rate, and smaller flake size after 6 h of shearing time result in weaker fibers. This trend is in line with what was observed in Raman spectroscopy of the solutions before spinning.

Morphology of the EG/FLG fibers was investigated by SEM. As illustrated in Figure 9a–h, the diameter of the fibers was maintained with longer shearing times in the TCR. The cross-sectional view suggests that the fibers became more packed with increasing shearing times. Comparing the EG/FLG fibers (Figure 9a–c,e–g) with CEG fibers (Figure 9d,h) reveals how the CEG fibers possess more porous morphology.

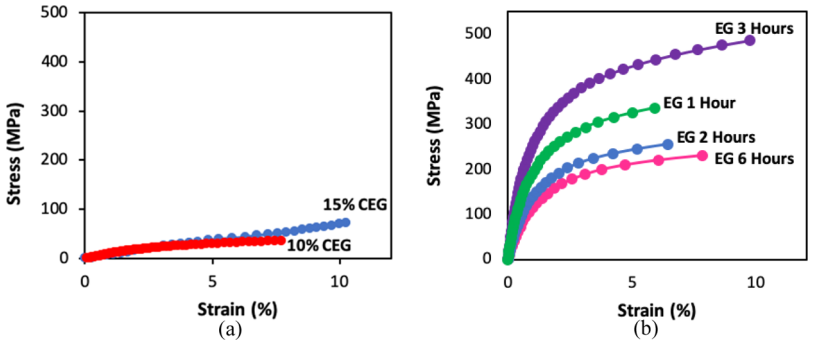

Figure 8. Mechanical properties of (a) CEG and (b) EG/FLG fibers.

https://dx.doi.org/10.1021/acsami.9b22824
ACS Appl. Mater. Interfaces XXXX, XXX, XXX−XXX

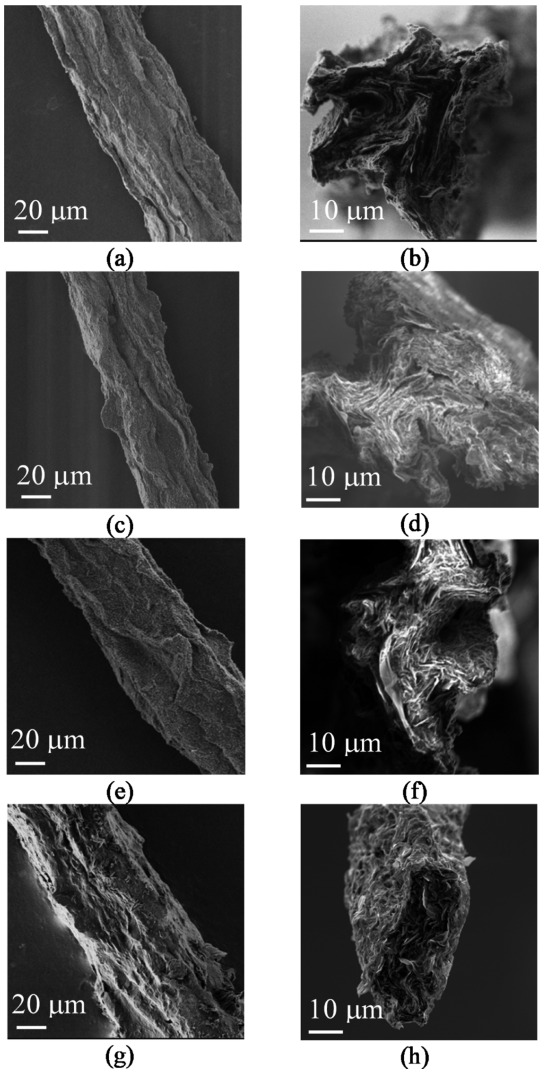

Figure 9. SEM micrographs of (a,b) EG/FLG 1 h, (c,d) EG/FLG 2 h, (e,f) EG/FLG 3 h, and (g,h) CEG fibers.

4. CONCLUSIONS

The expansion and exfoliation level of natural graphite particles using an aqueous solution and a TCR with a rotating outer cylinder and still inner cylinder was found to be determined by the shearing time in the TCR. This setup could potentially be used to expand and exfoliate graphite particles continuously by imposing an axial flow. In summary, the interlayer spacing in between graphene sheets increased with increasing shearing time. The level of expansion was found to be comparable to that of CEG particles. Moreover, the results obtained from XRD clearly show how structurally uniform the synthesized EG sample is in comparison to structurally inhomogeneous CEG particles. More importantly, a shearing time between 1 and 3 h resulted in almost no defects, which was essential for strong GFs. Shearing times exceeding 3 h resulted in an increase in graphene sheet exfoliation and the formation of structural defects on the graphene sheets. These defects could be used for nucleation on graphene sheets in energy storage and catalysis processes. Finally, the fibers fabricated using EG dispersions possessed noticeably better mechanical properties than fibers fabricated using CEG.

ASSOCIATED CONTENT

Supporting Information

The Supporting Information is available free of charge at https://pubs.acs.org/doi/10.1021/acsami.9b22824.

Additional results, including pH values of synthesized solutions, microscopy images, and size distribution (PDF)

AUTHOR INFORMATION

Corresponding Author

Yong Lak Joo − *Robert Fredrick Smith School of Chemical and Biomolecular Engineering, Cornell University, Ithaca, New York 14853, United States;* orcid.org/0000-0002-4646-1625; Phone: +1 607 255 8591; Email: ylj2@cornell.edu

Authors

Mohammed AlAmer − *Robert Fredrick Smith School of Chemical and Biomolecular Engineering, Cornell University, Ithaca, New York 14853, United States*

Somayeh Zamani − *Robert Fredrick Smith School of Chemical and Biomolecular Engineering, Cornell University, Ithaca, New York 14853, United States*

Kristi Fok − *Robert Fredrick Smith School of Chemical and Biomolecular Engineering, Cornell University, Ithaca, New York 14853, United States*

Aishwarya Satish − *Robert Fredrick Smith School of Chemical and Biomolecular Engineering, Cornell University, Ithaca, New York 14853, United States*

Ae Ran Lim − *Analytical Laboratory of Advanced Ferroelectric Crystals and Department of Science Education, Jeonju University, Jeonju 55069, South Korea*

Complete contact information is available at: https://pubs.acs.org/10.1021/acsami.9b22824

Author Contributions

Y.L.J. and M.A. conceived the project. M.A. and S.Z. designed the experiments. M.A. and K.F. performed FLG/EG synthesis. K.F. performed electrospraying and image analysis using optical microscopy and size distribution. M.A. and A.R.L. characterized the electrosprayed samples using XRD, Raman, and SEM and characterized the solution using a Zetasizer. S.Z. and A.S. performed fiber fabrication using electrospinning. S.Z. characterized the produced fibers. All authors analyzed the data and discussed the experimental plans. M.A. wrote the manuscript, and all authors commented and revised it. Y.L.J. supervised the whole project.

Funding

M.A. acknowledges Saudi Aramco's Advanced Degree Program. This research was also supported by the Basic Science Research program through the National Research Foundation of Korea (NRF), funded by the Ministry of Education (2018R1D1A1B07041593).

Notes

The authors declare no competing financial interest.

ACKNOWLEDGMENTS

This work made use of the Cornell Center of Materials Research Shared Facilities, which are supported through the NSF MRSEC program (DMR-1719875). The authors acknowledge the Cornell Laboratory of Atomic and Solid-

State Physics Machine Shop for manufacturing the TCR setup and Asbury Carbons for providing graphite samples.

REFERENCES

(1) Mayorov, A. S.; Gorbachev, R. V.; Morozov, S. V.; Britnell, L.; Jalil, R.; Ponomarenko, L. A.; Blake, P.; Novoselov, K. S.; Watanabe, K.; Taniguchi, T.; Geim, A. K. Micrometer-Scale Ballistic Transport in Encapsulated Graphene at Room Temperature. *Nano Lett.* **2011**, *11*, 2396−2399.
(2) Lee, C.; Wei, X.; Kysar, J. W.; Hone, J. Measurement of the Elastic Properties and Intrinsic Strength of Monolayer Graphene. *Science* **2008**, *321*, 385−388.
(3) Balandin, A. A. Thermal Properties of Graphene and Nanostructured Carbon Materials. *Nat. Mater.* **2011**, *10*, 569−581.
(4) Geim, A. K.; Novoselov, K. S. The Rise of Graphene. *Nat. Mater.* **2007**, *6*, 183−191.
(5) Stankovich, S.; Dikin, D. A.; Dommett, G. H. B.; Kohlhaas, K. M.; Zimney, E. J.; Stach, E. A.; Piner, R. D.; Nguyen, S. T.; Ruoff, R. S. Graphene-Based Composite Materials. *Nature* **2006**, *442*, 282−286.
(6) Serp, P.; Corrias, M.; Kalck, P. Carbon Nanotubes and Nanofibers in Catalysis. *Appl. Catal., A* **2003**, *253*, 337−358.
(7) Liu, C.; Li, F.; Ma, L.-P.; Cheng, H.-M. Advanced Materials for Energy Storage. *Adv. Mater.* **2010**, *22*, E28−E62.
(8) Hassan, F. M.; Elsayed, A. R.; Chabot, V.; Batmaz, R.; Xiao, X.; Chen, Z. Subeutectic Growth of Single-Crystal Silicon Nanowires Grown on and Wrapped with Graphene Nanosheets: High-Performance Anode Material for Lithium-Ion Battery. *ACS Appl. Mater. Interfaces* **2014**, *6*, 13757−13764.
(9) Fei, L.; Yoo, S. H.; Villamayor, R. A. R.; Williams, B. P.; Gong, S. Y.; Park, S.; Shin, K.; Joo, Y. L. Graphene Oxide Involved Air-Controlled Electrospray for Uniform, Ultrafast, Instantly-Dry, and Binder-Free Electrode Fabrication. *ACS Appl. Mater. Interfaces* **2017**, *9*, 9738−9746.
(10) Cheng, Q.; Tang, J.; Ma, J.; Zhang, H.; Shinya, N.; Qin, L.-C. Graphene and Nanostructured Mno2 Composite Electrodes for Supercapacitors. *Carbon* **2011**, *49*, 2917−2925.
(11) Elzatahry, A. A.; Abdullah, A. M.; El-Din, T. A. S.; Al-Enizi, A. M.; Maarouf, A. A.; Galal, A.; Hassan, H. K.; El-Ads, E. H.; Al-Theyab, S. S.; Al-Ghamdi, A. A. Nanocomposite Graphene-Based Material for Fuel Cell Applications. *Int. J. Electrochem. Sci.* **2012**, *7*, 3115−3126.
(12) Lee, J.; Tao, L.; Hao, Y.; Ruoff, R. S.; Akinwande, D. Embedded-Gate Graphene Transistors for High-Mobility Detachable Flexible Nanoelectronics. *Appl. Phys. Lett.* **2012**, *100*, 152104.
(13) Reina, A.; Jia, X.; Ho, J.; Nezich, D.; Son, H.; Bulovic, V.; Dresselhaus, M. S.; Kong, J. Large Area, Few-Layer Graphene Films on Arbitrary Substrates by Chemical Vapor Deposition. *Nano Lett.* **2009**, *9*, 30−35.
(14) Berger, C.; Song, Z.; Li, T.; Li, X.; Ogbazghi, A. Y.; Feng, R.; Dai, Z.; Marchenkov, A. N.; Conrad, E. H.; First, P. N.; de Heer, W. A. Ultrathin Epitaxial Graphite: 2d Electron Gas Properties and a Route toward Graphene-Based Nanoelectronics. *J. Phys. Chem. B* **2004**, *108*, 19912−19916.
(15) Novoselov, K. S.; Jiang, D.; Schedin, F.; Booth, T. J.; Khotkevich, V. V.; Morozov, S. V.; Geim, A. K. Two-Dimensional Atomic Crystals. *Proc. Natl. Acad. Sci. U.S.A.* **2005**, *102*, 10451−10453.
(16) Gao, X.; Jang, J.; Nagase, S. Hydrazine and Thermal Reduction of Graphene Oxide: Reaction Mechanisms, Product Structures, and Reaction Design. *J. Phys. Chem. C* **2010**, *114*, 832−842.
(17) Bai, H.; Li, C.; Shi, G. Functional Composite Materials Based on Chemically Converted Graphene. *Adv. Mater.* **2011**, *23*, 1089−1115.
(18) Park, W. K.; Kim, H.; Kim, T.; Kim, Y.; Yoo, S.; Kim, S.; Yoon, D. H.; Yang, W. S. Facile Synthesis of Graphene Oxide in a Couette-Taylor Flow Reactor. *Carbon* **2015**, *83*, 217−223.
(19) AlAmer, M.; Lim, A. R.; Joo, Y. L. Continuous Synthesis of Structurally Uniform Graphene Oxide Materials in a Model Taylor-Couette Flow Reactor. *Ind. Eng. Chem. Res.* **2019**, *58*, 1167−1176.
(20) Tran, T. S.; Park, S. J.; Yoo, S. S.; Lee, T.-R.; Kim, T. High Shear-Induced Exfoliation of Graphite into High Quality Graphene by Taylor-Couette Flow. *RSC Adv.* **2016**, *6*, 12003−12008.
(21) Taylor, G. I. Stability of a Viscous Liquid Contained between Two Rotating Cylinders. *Proc. R. Soc. London* **1923**, *102*, 541−542.
(22) Couette, M. Distinction De Deux Régimes Dans Le Mouvement Des Fluids. *J. Phys. Theor. Appl.* **1890**, *9*, 414−424.
(23) Grossmann, S.; Lohse, D.; Sun, C. High-Reynolds Number Taylor-Couette Turbulence. *Annu. Rev. Fluid. Mech.* **2016**, *48*, 53−80.
(24) Yoshimoto, S.; Amano, J.; Miura, K. Synthesis of a Fullerene/Expanded Graphite Composite and Its Lubricating Properties. *J. Mater. Sci.* **2010**, *45*, 1955−1962.
(25) Makotchenko, V. G.; Grayfer, E. D.; Nazarov, A. S.; Kim, S.-J.; Fedorov, V. E. The Synthesis and Properties of Highly Exfoliated Graphites from Fluorinated Graphite Intercalation Compounds. *Carbon* **2011**, *49*, 3233−3241.
(26) Lecuyer, A. P.; Luche, J. L.; Kagan, H. B.; Colin, G.; Mazieres, C. In Graphit Eingelagertes Brom, Ein Festes Bromierungsagenz in Der Organischen Chemie. *Chem. Informationsdienst* **1973**, *4*, 1690−1692.
(27) Viculis, L. M.; Mack, J. J.; Mayer, O. M.; Hahn, H. T.; Kaner, R. B. Intercalation and Exfoliation Routes to Graphite Nanoplatelets. *J. Mater. Chem.* **2005**, *15*, 974−978.
(28) Li, J.-h.; Liu, Q.; Da, H.-f. Preparation of Sulfur-Free Exfoliated Graphite at a Low Exfoliation Temperature. *Mater. Lett.* **2007**, *61*, 1832−1834.
(29) Xiling, C.; Kemin, S.; Jihui, L.; Jinpeng, L. Preparation of Lower-Sulfur Content and Expandable Graphite. *Carbon* **1996**, *34*, 1599−1600.
(30) Furdin, G. Exfoliation Process and Elaboration of New Carbonaceous Materials. *Fuel* **1998**, *77*, 479−485.
(31) Jiang, B.; Tian, C.; Wang, L.; Xu, Y.; Wang, R.; Qiao, Y.; Ma, Y.; Fu, H. Facile Fabrication of High Quality Graphene from Expandable Graphite: Simultaneous Exfoliation and Reduction. *Chem. Commun.* **2010**, *46*, 4920−4922.
(32) Hung, W.-C.; Wu, K.-H.; Lyu, D.-Y.; Cheng, K.-F.; Huang, W.-C. Preparation and Characterization of Expanded Graphite/Metal Oxides for Antimicrobial Application. *Mater. Sci. Eng., C* **2017**, *75*, 1019−1025.
(33) Li, J.; Li, J.; Li, M. Preparation of Expandable Graphite with Ultrasound Irradiation. *Mater. Lett.* **2007**, *61*, 5070−5073.
(34) McAllister, M. J.; Li, J.-L.; Adamson, D. H.; Schniepp, H. C.; Abdala, A. A.; Liu, J.; Herrera-Alonso, M.; Milius, D. L.; Car, R.; Prud'homme, R. K.; Aksay, I. A. Single Sheet Functionalized Graphene by Oxidation and Thermal Expansion of Graphite. *Chem. Mater.* **2007**, *19*, 4396−4404.
(35) Tryba, B.; Morawski, A. W.; Inagaki, M. Preparation of Exfoliated Graphite by Microwave Irradiation. *Carbon* **2005**, *43*, 2417−2419.
(36) Janowska, I.; Chizari, K.; Ersen, O.; Zafeiratos, S.; Soubane, D.; Costa, V. D.; Speisser, V.; Boeglin, C.; Houllé, M.; Bégin, D.; Plee, D.; Ledoux, M.-J.; Pham-Huu, C. Microwave Synthesis of Large Few-Layer Graphene Sheets in Aqueous Solution of Ammonia. *Nano Res.* **2010**, *3*, 126−137.
(37) Qian, W.; Hao, R.; Hou, Y.; Tian, Y.; Shen, C.; Gao, H.; Liang, X. Solvothermal-Assisted Exfoliation Process to Produce Graphene with High Yield and High Quality. *Nano Res.* **2009**, *2*, 706−712.
(38) Chung, D. D. L. Exfoliation of Graphite. *J. Mater. Sci.* **1987**, *22*, 4190−4198.
(39) Xu, Z.; Gao, C. Graphene Chiral Liquid Crystals and Macroscopic Assembled Fibres. *Nat. Commun.* **2011**, *2*, 571.
(40) Xu, Z.; Gao, C. Graphene Fiber: A New Trend in Carbon Fibers. *Mater. Today* **2015**, *18*, 480−492.
(41) Cong, H.-P.; Ren, X.-C.; Wang, P.; Yu, S.-H. Wet-Spinning Assembly of Continuous, Neat, and Macroscopic Graphene Fibers. *Sci. Rep.* **2012**, *2*, 613.
(42) Chen, Y.; Guo, F.; Jachak, A.; Kim, S.-P.; Datta, D.; Liu, J.; Kulaots, I.; Vaslet, C.; Jang, H. D.; Huang, J.; Kane, A.; Shenoy, V. B.;

https://dx.doi.org/10.1021/acsami.9b22824
ACS Appl. Mater. Interfaces XXXX, XXX, XXX−XXX

Hurt, R. H. Aerosol Synthesis of Cargo-Filled Graphene Nanosacks. *Nano Lett.* **2012**, *12*, 1996−2002.
(43) Xu, W.; Kwok, K. S.; Gracias, D. H. Ultrathin Shape Change Smart Materials. *Acc. Chem. Res.* **2018**, *51*, 436−444.
(44) Reynolds, M. F.; McGill, K. L.; Wang, M. A.; Gao, H.; Mujid, F.; Kang, K.; Park, J.; Miskin, M. Z.; Cohen, I.; McEuen, P. L. Capillary Origami with Atomically Thin Membranes. *Nano Lett.* **2019**, *19*, 6221−6226.
(45) Patra, N.; Wang, B.; Král, P. Nanodroplet Activated and Guided Folding of Graphene Nanostructures. *Nano Lett.* **2009**, *9*, 3766−3771.
(46) Williams, B. P.; Pinge, S.; Kim, Y.-K.; Kim, J.; Joo, Y. L. Enhanced Dispersion and Stability of Petroleum Coke Water Slurries Via Triblock Copolymer and Xanthan Gum: Rheological and Adsorption Studies. *Langmuir* **2015**, *31*, 8989−8997.
(47) Eckmann, A.; Felten, A.; Mishchenko, A.; Britnell, L.; Krupke, R.; Novoselov, K. S.; Casiraghi, C. Probing the Nature of Defects in Graphene by Raman Spectroscopy. *Nano Lett.* **2012**, *12*, 3925−3930.

https://dx.doi.org/10.1021/acsami.9b22824
ACS Appl. Mater. Interfaces XXXX, XXX, XXX−XXX